Beyond the Gouy−Chapman Model with Heterodyne-Detected Second Harmonic Generation

Paul E. Ohno,[†] HanByul Chang,[†] Austin P. Spencer,[†] Yangdongling Liu,[†] Mavis D. Boamah,[†] Hong-fei Wang,[‡] and Franz M. Geiger*,[†]

[†]Department of Chemistry, Northwestern University, 2145 Sheridan Road, Evanston, Illinois 60208, United States
[‡]Department of Chemistry and Shanghai Key Laboratory of Molecular Catalysis and Innovative Materials, Fudan University, Shanghai 200433, China

S *Supporting Information*

ABSTRACT: We report ionic strength-dependent phase shifts in second harmonic generation (SHG) signals from charged interfaces that verify a recent model in which dispersion between the fundamental and second harmonic beams modulates observed signal intensities. We show how phase information can be used to unambiguously separate the $\chi^{(2)}$ and interfacial potential-dependent $\chi^{(3)}$ terms that contribute to the total signal and provide a path to test primitive ion models and mean field theories for the electrical double layer with experiments to which theory must conform. Finally, we demonstrate the new method on supported lipid bilayers and comment on the ability of our new instrument to identify hyper-Rayleigh scattering contributions to common homodyne SHG measurements in reflection geometries.
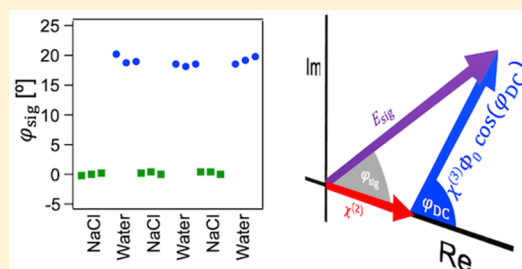
The application of second harmonic generation (SHG) and sum frequency generation (SFG) to charged aqueous interfaces has been an area of substantial interest for several decades.[1−9] The field has been greatly influenced by the foundational work of Eisenthal and co-workers,[1] who interpreted the SHG signal generated from the fused silica/water interface, E_{SHG}, as consisting of a second-order component, $\chi^{(2)}$, and an interfacial potential-dependent third-order component, $\chi^{(3)}$, using the following model 1

$$E_{SHG} \propto \chi^{(2)} + \chi^{(3)}\Phi(0) \quad (1)$$

Here, $\Phi(0)$ is the interfacial potential present at the zero plane of the interface, referenced to zero potential in the bulk solution. The $\chi^{(2)}$ term in eq 1 originates from molecules that are net oriented at the interface. The interfacial potential-dependent $\chi^{(3)}$ term is present at charged interfaces due to the presence of a static (DC) E-field generated by the surface charge and primarily results from the reorientation and polarization of water molecules in response to the static E-field.[10] Because the penetration of the static E-field from the surface into the aqueous solution depends on the electrostatic screening within the electrical double layer (EDL), the Eisenthal $\chi^{(3)}$ effect makes SHG and, analogously, SFG sensitive probes of interfacial potential and EDL structure.

Many attempts have been made to disentangle the $\chi^{(2)}$ and $\chi^{(3)}$ contributions.[11−18] A recent study of ours identified the $\chi^{(3)}$ contribution to be of bulk origin.[19] Around the same time, Tian and co-workers[6] and Roke and co-workers[7] updated the purely additive model 1[1,20−23] to account for the optical dispersion between the fundamental and second harmonic/sum frequency wavelengths within the interfacial region. For

an electrostatic potential exponentially decaying with distance z from the interface with a Debye screening length λ_D, $\Phi(z) \propto e^{-z\lambda_D^{-1}}$, the interference between the signal generated at different depths away from the interface results in the now firmly established model 2[6,7,10,19,24−28]

$$E_{SHG} \propto \chi^{(2)} + \chi^{(3)}\Phi(0) \cos(\varphi) e^{i\varphi} \quad (2)$$

with the phase angle, φ, of the $\chi^{(3)}$ term taking the exact solution (derivation of this form can be found in the SI, section 1)[19,24−26,28]

$$\varphi = \arctan(\Delta k_z \lambda_D) \quad (3)$$

where Δk_z is the wavevector mismatch of the optical process (calculation of Δk_z can be found in the SI, section 2). We now report phase measurements obtained using a new instrument that we analyze using model 2 so as to unambiguously separate the $\chi^{(2)}$ and interfacial potential-dependent $\chi^{(3)}$ terms. The results provide a path to test primitive ion models and mean field theories for the EDL with experiments to which theory must conform. Moreover, the approach advances the utility of SHG from charged interfaces as an "optical voltmeter".[29] Finally, we demonstrate the new method on supported lipid bilayers and comment on the ability of our new instrument to identify hyper-Rayleigh scattering contributions to common homodyne SHG measurements in reflection geometries.

The phase angle φ in model 2 is not the phase inherent to $\chi^{(3)}$, which varies when $\chi^{(3)}$ is on- or near-resonance. Rather, φ results from the fact that the DC-field-induced $\chi^{(3)}$ signal is generated throughout a range of depths away from the interface. For clarity, we will subsequently label this phase angle the DC phase angle, φ_{DC}, in order to distinguish it from the phase of the overall signal, φ_{sig}, measured in the subsequently described experiment using α-quartz against 100 mM NaCl as a reference state. We see from eq 3 that φ_{DC} is a function of the ionic strength of the bulk solution (which determines the Debye screening length) and the wavelengths and angles of the input and output beams. The result of the interference is both a modulation of the amplitude of the $\chi^{(3)}$ term and a shift in its phase as ionic strength is varied. Simply put, when detecting intensities, eqs 2 and 3 show that the coefficient "+1" in model 1 instead varies between −1 and 1, depending on the ionic strength of the aqueous solution or the sign and magnitude of the surface charge density, as is taken into account in model 2.

In the case of nonresonant SHG measurements, the inherent phases of $\chi^{(2)}$ and $\chi^{(3)}$ are expected to be purely real, i.e., precisely in phase (0°) or out of phase (180°) with respect to the excitation field. However, eq 2 makes it clear that the overall DC-field-induced $\chi^{(3)}$ term can still be phase-shifted relative to the $\chi^{(2)}$ contribution. Our earlier study[19] showed constructive and destructive interference between the surface and bulk terms from the α-quartz/water interface, which, due to the inherent 90° phase shift between surface and bulk terms derived from Maxwell's equations,[30,31] would not be expected according to eq 1 when $\chi^{(2)}$ and $\chi^{(3)}$ are purely real. This interference was explained by the phase factor included in eq 2, and the measurements provided experimental evidence for the validity and importance of eqs 2 and 3. However, at that time, we made no attempt to quantify the phase shift nor deduce what additional information its measurement can provide, which we report here now.

Standard (homodyne) SHG experiments measure only the intensity of the SHG signal, not its phase. Heterodyne-detected SHG (HD-SHG), capable of resolving phase, requires interference between the SHG signal and SHG generated from a reference, called the local oscillator (LO).[32] The phase information encoded is then recovered in the time domain by varying the phase between the signal and LO through the use of a phase shifting unit (PSU).[33] Prior reports of HD-SHG have been largely limited to condensed matter bound by nondispersive media.[31,34−38] In contrast, determining the phase of the signal generated at a buried interface such as fused silica/water is challenging due to the spatial and temporal dispersion between the fundamental beam and SHG signal as they both propagate away from the interface. This dispersion complicates the generation of a LO that must be collinear and co-temporal with the signal in order for the signal and LO to propagate together and interfere at the detector. The correction of spatial dispersion has been demonstrated through the use of compensating prisms,[39] though this correction does not address temporal dispersion, which represents a significant challenge as even a few mm of glass can be enough to reduce or completely eliminate temporal overlap.

We earlier demonstrated[40] a SHG phase measurement from the fused silica/water interface by using a hemisphere to avoid refraction of the beams exiting the sample, recollimating the fundamental and SHG beams close to the hemisphere to minimize spatial dispersion, and detecting the signal through a monochromator, which stretches the pulses in time and can make up for some loss of temporal overlap. However, likely because the poor temporal overlap caused by dispersion in the hemisphere was not directly addressed in that study, the efficiency of the interference was low, resulting in a low signal-to-noise ratio and rendering the detection of the small phase shifts expected from changes in φ_{DC} difficult or impossible.

In this Letter, we report SHG phase measurements from the fused silica/water interface with a significantly improved signal-to-noise in order to directly measure phase shifts that occur due to changing EDL thickness. We correct for the temporal dispersion caused by the fused silica hemisphere with a calcite time delay compensator (TDC) and minimize spatial dispersion and chromatic aberration by recollimating with an achromatic off-axis parabolic (OAP) mirror (see the SI, section 3, for calculations of the spatial and temporal dispersion in our setup). We utilize a "sample-first" geometry and generate the LO in a 50 μm z-cut α-quartz plate. With this HD-SHG instrument, we directly measure phase shifts in the SHG signal from the fused silica/water interface at different ionic strengths, as predicted by eq 2.

The instrument is designed such that homodyne SHG is readily measured in the same setup as HD-SHG through removal of the reference α-quartz crystal (see the schematic in Figure 1). Homodyne SHG control studies measured in this
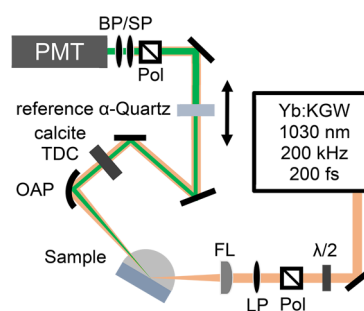

Figure 1. Schematic of PR-SHG instrument. $\lambda/2$ = half-waveplate, Pol = polarizer, LP = long-pass filter, FL = focusing lens, OAP = off-axis parabolic mirror, TDC = time delay compensator, SP = short-pass filter, BP = band-pass filter, PMT = photomultiplier tube. The reference α-quartz crystal is mounted on a 100 mm translational stage. Part numbers and specifics are provided in SI section 6.

way show the expected quadratic dependence of detected signal intensity on input power as well as the expected narrow bandwidth of the detected signal centered around the second harmonic wavelength of our fundamental beam (SI, section 4).

We next show that the HD-SHG instrument yields the expected interference between the signal and LO. Figure 2A shows that the homodyne I_{SHG} from the fused silica/water interface is low. Addition of the α-quartz crystal amplifies the I_{SHG} considerably due to generation of the LO, while translation of the crystal along the beam path generates an interference pattern. Rotating the reference crystal azimuthally by 60°, which changes the phase of the LO by 180°, inverts the interference pattern. Without the calcite TDC plate present and aligned such that it re-overlaps the fundamental and SHG pulses in time prior to their incidence upon the α-quartz crystal, no interference is seen as the crystal is translated, demonstrating the importance of the TDC in the experimental setup.
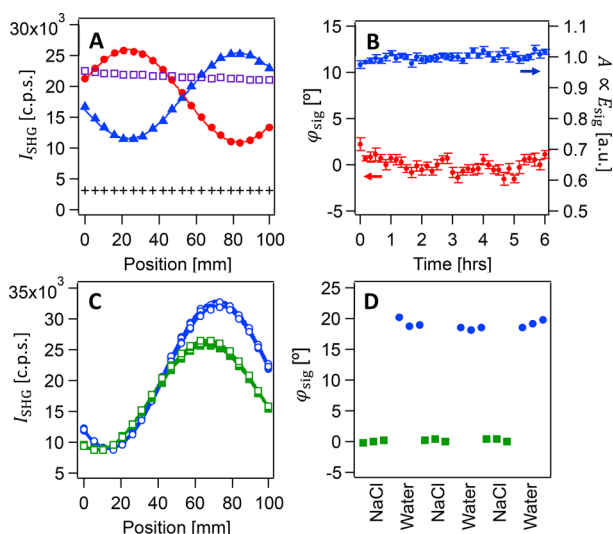
Figure 2. HD-SHG Measurements. (A) Homodyne SHG measurement (+) and interference patterns (● and ▲) with fits from the fused silica/100 mM NaCl interface. The phase of the LO for the blue trace has been shifted by 180°. Without the TDC, no interference is seen (□). Fits can be found in Table S2. (B) Stability of the measurement over time. The phase is shown in red, and A, proportional to E_{sig}, is shown in blue. (C) Interference patterns and fits from cycling between 100 mM NaCl (□) and 2 μM air-equilibrated water, pH 5.8 (○). (D) φ_{sig} extracted from the fits in (C) shows a reversible phase shift of 19.1 ± 0.4° at pH 5.8.

The phase extracted from the HD-SHG measurements remains stable over the course of hours, as demonstrated in Figure 2B, most likely due to our chosen collinear geometry as changes in shared optics affect both beam paths equally. However, small shifts in beam pointing or sample position will lead to differing path lengths through the dispersive fused silica hemisphere, causing phase drift. Indeed, we noted a consistent phase drift of ~10° over 2 h immediately following the hemisphere being clamped to the stage, attributed here to structural relaxation of the flow/optical cell assembly that results in small (μm-scale) changes in the position of the clamped hemisphere with respect to the beam path. However, after this initial relaxation period, Figure 2B shows <±2° phase drifts over 6 h, with amplitude measurements that fluctuate by ~2%. As individual scans take only 5 min, phase measurements taken in succession can be made with a precision of better than 1°.

Equation 2 predicts a difference in the phase of E_{sig} from a fused silica substrate in contact with 2 μM air-equilibrated water vs 100 mM NaCl, with the exact magnitude of this phase shift determined by the relative amplitudes of the $\chi^{(3)}$ and $\chi^{(2)}$ terms. Though our previous study[19] showed evidence for the existence of this phase shift, we were not able to directly measure its magnitude at that time. With our new HD-SHG setup, we detect a clear phase shift of 2 μM air-equilibrated water relative to 100 mM NaCl, shown in Figure 2C,D (triplicate measurement in three successions). The measurements give $\varphi_{sig,2\mu M} = 19.1 \pm 0.4°$ and serve as direct evidence that the phase shift expressed in eq 2 must be taken into account when SHG and SFG are generated from interfaces at low ionic strengths.

Separation of $\chi^{(2)}$ and $\chi^{(3)}$ contributions from the detected signal intensity in order to use SHG as an optical voltmeter has been a long-standing goal. Previously, without phase

information, it was impossible to determine if the observed changes in E_{sig} resulted from changes in the $\chi^{(2)}$ term, the $\chi^{(3)}$ potential-dependent term, or both. We now demonstrate how this goal is experimentally attainable using HD-SHG. Figure 3A shows φ_{sig} and E_{sig} extracted from phase measurements like
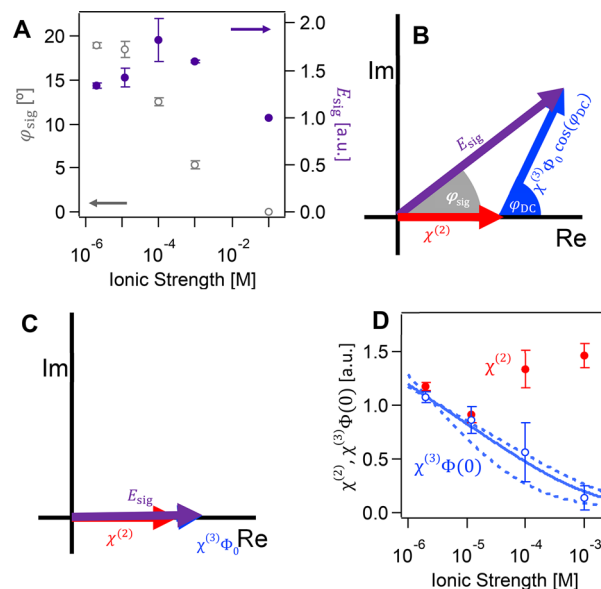

Figure 3. Separation of $\chi^{(2)}$ and $\chi^{(3)}$ terms. (A) φ_{sig} (gray) and E_{sig} (purple) extracted from fits as a function of ionic strength (pH = 5.8). Error bars represent the standard deviation from three consecutive measurements. (B) Graphic representation of real and imaginary components of the signal field at low ionic strength. Because $\chi^{(2)}$ and $\chi^{(3)}$ are themselves purely real, any phase shift can be attributed to φ_{DC} according to eq 2. (C) Graphic representation of the signal field at high ionic strength, where the phase shift is minimal and the overall signal remains nearly entirely real. (D) $\chi^{(2)}$ and $\chi^{(3)}\Phi_0$ calculated from the data in (A) according to eqs 4A and 4B, pH = 5.8.

the ones shown in Figure 2 carried out as a function of ionic strength. E_{sig} initially increases upon addition of salt before decreasing at high ionic strength, consistent with SHG intensity (I_{SHG}) measurements reported previously.[28,41] Yet, here we report the amplitude of this response (E_{sig}) from the HD-SHG measurement, not merely by square rooting I_{SHG}.

The optical process is illustrated in a vector diagram of the signal field in the complex plane, shown in Figure 3B. The phase, φ_{sig}, and amplitude of the sample SHG, E_{sig}, are the experimental observables extracted from the measured interference patterns and are shown in gray and purple, respectively, corresponding to the symbol colors used in Figure 3A. Following eq 2, E_{sig} is modeled to be the sum of a $\chi^{(2)}$ term (shown in red and purely real in our nonresonant experiments) and a $\chi^{(3)}\Phi(0)$ term (shown in blue), whose phase and amplitude are modulated by φ_{DC}. From trigonometry, we find that

$$\chi^{(3)}\Phi(0) = \frac{\sin(\varphi_{sig})E_{sig}}{\cos(\varphi_{DC})\sin(\varphi_{DC})} \tag{4A}$$

$$\chi^{(2)} = \cos(\varphi_{sig})E_{sig} - \cos^2(\varphi_{DC})\chi^{(3)}\Phi_0 \tag{4B}$$

Here, every factor on the right side of eq 4A is measured (E_{sig}, φ_{sig}) or can be calculated (φ_{DC}), and once this is determined, the same holds true for eq 4B. Thus, with the additional phase

information from HD-SHG measurements, we disentangle the $\chi^{(3)}\Phi(0)$ and $\chi^{(2)}$ terms from E_{sig}, provided we know the Debye screening length.

Given the experimental[6] and computational[27] evidence that at constant temperature $\chi^{(3)}$ is invariant with the exact nature of the interface and constant across a wide range of aqueous phase conditions up to 100 mM ionic strength, we can interpret the $\chi^{(3)}\Phi(0)$ term as being directly proportional to the interfacial potential without having to rely on a model such as Gouy−Chapman or assuming a priori that $\chi^{(2)}$ remains constant, as previous studies have posited. Yet, our analysis relies on φ_{DC} being large enough such that the overall phase shift, φ_{sig}, can be reliably detected. Figure 3C illustrates the case of moderate to high ionic strengths (>∼10 mM in our reflection geometry), where the overall signal is nearly entirely real. Considering the noise performance of our instrument illustrated in Figure 2B, it is not feasible to measure phase shifts of <∼1° at this time and to separate the $\chi^{(2)}$ and $\chi^{(3)}$ components at high ionic strength. However, for <∼1 mM ionic strength, the phase shift is large enough to measure and separate the terms according to eqs 4A and 4B. The results of this separation are shown in Figure 3D, which shows that $\chi^{(3)}\Phi(0)$ decreases significantly with increasing ionic strength, attributable to increased screening within the EDL as the concentration of ions increases. In contrast, $\chi^{(2)}$ remains comparatively constant across 3 orders of magnitude of ionic strength, though changes on the order of ∼30% are seen. Note that the magnitude of the uncertainties on the point estimates is largely due to error propagation according to eqs 4A and 4B. The best fit of $\chi^{(3)}\Phi(0)$ with the Gouy−Chapman model yields a surface charge density of −0.0024(18) C/m² and is represented by the blue line in Figure 3D, which agrees well with the measured data. As expected, the charge density for pH 5.8 is smaller than what has been published for pH 7,[14,22] given that the point of zero charge for fused silica is ∼2.5.[42]

Our findings support the conclusion that we have successfully separated out the $\chi^{(3)}\Phi(0)$ term without relying on the Gouy−Chapman model. Measurements of E_{sig} referenced to the E_{sig} generated from an interface with a known $\chi^{(2)}$ value, such as α-quartz, are now needed to obtain $\Phi(0)$ absolutely, without the use of Gouy−Chapman theory or any other model for the interfacial potential. The method therefore opens the possibility to test primitive ion models or mean field theories for aqueous interfaces directly and without externally applied labels.

On a slightly different albeit highly relevant note, we mention at this point a recent investigation by Dreier et al.[43] into the surface potential of charged lipid monolayer/water interfaces in which seemingly different results were obtained between homodyne nonresonant SHG measurements and chemically specific SFG measurements of the OH stretching region. Part of this difference was attributed to hyper-Rayleigh scattering (HRS) contributions to the detected SHG intensity. As HRS is produced incoherently, any HRS emitted from the sample—while it may be present in the homodyne measurements—would not contribute to the interference from which the amplitude and phase of the signal SHG are extracted in HD-SHG. Thus, our HD-SHG measurements are free from any potential convolution with HRS. Indeed, our HD-SHG apparatus should be ideal for separating out any possible contributions of HRS to the SHG signal generated from any interface. To test this idea, we obtained E_{sig} from supported lipid bilayer/water interfaces as a function of ionic strength

measured with different instruments (Figure 4). In addition to the HD-SHG measurements that yield E_{sig} by phase-
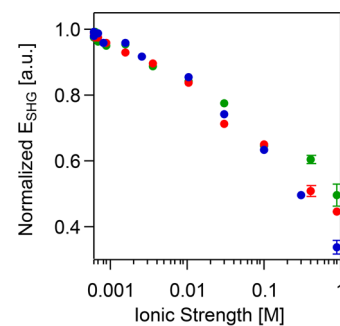

Figure 4. Homodyne- and HD-SHG comparison. Comparison of E_{sig} derived from homodyne (SHG λ = 400 nm: green ●; 515 nm: red ●) and HD-SHG (515 nm: blue ●) measurements from a supported lipid bilayer/water interface as a function of ionic strength. The greater amplitude detected by the homodyne measurements at high ionic strength is consistent with the presence of HRS. Error bars are derived from repeat measurements.

referencing, we obtained E_{sig} by square rooting homodyne-detected I_{SHG} signals with the same laser system as well as with an 800 nm Ti:sapphire oscillator system described previously.[19] The three measurements track each other closely at low ionic strength (<100 mM), while at high ionic strength (approaching 1 M), both homodyne measurements indicate a higher $E_{sig} = \sqrt{I_{SHG}}$ than the E_{sig} obtained from the HD-SHG measurement through model 2 ($E_{sig} \propto A$ from eqs 5 and 6, vide infra). Additionally, the 400 nm homodyne measurement indicates more signal than the 515 nm measurement, which would be expected as shorter wavelengths produce a greater HRS intensity.[44] We caution that our observations are not conclusive evidence for the presence of HRS in homodyne SHG in reflection geometries such as the ones employed here and elsewhere, yet this result is consistent with its presence and will be the subject of future studies.

In conclusion, we have demonstrated an experimental apparatus capable of measuring the phase of SHG signals from buried interfaces. We used this apparatus to measure the phase shift in SHG generated at the fused silica/water interface as a function of ionic strength, a direct result of charge screening compressing the width of the EDL as the ionic strength increases. Furthermore, we showed how this additional phase information can be used to unambiguously separate the $\chi^{(2)}$ and $\chi^{(3)}$ contributions to detected SHG from charged interfaces, a long-standing goal in the field. While model 2 was successfully applied to the experimental data, we caution that the analysis relies on three assumptions: (a) the nonlinear optical signal recorded at the detector consists of only second- and third-order terms, (b) the surface potential decays exponentially with distance, and (c) Debye−Hückel theory is applicable for the Debye length.

We envision several avenues of future study in which the instrument described here can be impactful. In one avenue, determination of the absolute magnitude of the $\chi^{(2)}$ and $\chi^{(3)}$ components could be made through comparison with a known absolute reference, similar to the approach used in heterodyne SFG spectroscopy. This comparison, in combination with isolation of the $\chi^{(3)}$ contribution described here, would allow for direct, optical quantification of the surface potential at

oxide/water interfaces, without relying on the Gouy–Chapman model or the assumption that $\chi^{(2)}$ remains constant. In another avenue, we foresee coupling the phase measurements described in this study with a system containing an electrode under potential control. By controlling the potential and thus the magnitude of the $\chi^{(3)}$ contribution, the comparison of observed phase shifts with the phase shifts predicted by model 2 would open an experimental window into how accurate theoretical (atomistic or coarse-grain simulations) and model (primitive ions, continuum models, or mean field theory) predictions of the EDL are. Despite our advance, we caution that physics and chemistry not described in model 2 may contribute to the signal generation process in ways that remain to be uncovered.

EXPERIMENTAL SECTION

A detailed description of the optical setup as well as sample and solution preparation can be found in the SI, section 6. HD-SHG requires interference between the sample SHG signal and the LO generated in an α-quartz crystal. The detected total signal intensity, I_{SHG}, produced by the coherent interference between the signal and LO is governed by the following equation[33]

$$I_{SHG} \propto |E_{sig} + E_{LO}|^2 = |E_{sig}|^2 + |E_{LO}|^2$$
$$+ 2E_{sig}E_{LO}\alpha \cos(\varphi_{sig} - \varphi_{LO} + \varphi_{PSU}) \qquad (5)$$

where α is the overlap parameter that represents the degree of spatial and temporal overlap between the two beams, φ_{sig} and φ_{LO} represent the phases of the signal and LO, respectively, and φ_{PSU} represents the additional phase shift introduced by the PSU. We vary φ_{PSU} by translating the reference α-quartz crystal along the beam path, taking advantage of the slight optical dispersion in air, according to the following equation,[40] $l_0 = \lambda/2\Delta n$, where l_0 is the translation distance required for one period of oscillation, λ is the fundamental wavelength, and Δn is the difference in refractive index between the fundamental and SHG wavelengths. Using data from the literature[45] for the refractive index of our 1030 and 515 nm beams in air, we calculate l_0 to be ~114 mm. Thus, with a 100 mm translational stage, we are able obtain an interference pattern of just less than one full period of oscillation with our PSU. The time required for each scan depends on the number of points that the 100 mm range of the stage is divided into as well as the length of acquisition at each point. A typical scan of 20 points at 10 s per point took ~5 min.

Scanning the position of the α-quartz crystal shifts the phase between the signal and LO and results in an interference pattern in I_{SHG} as a function of stage position. We fit the interference pattern to the following equation

$$I_{SHG} = I_0 + A \cos(fx + \varphi_{fit}) \qquad (6)$$

where x is the stage position and I_0, A, f, and φ_{fit} are parameters free to be optimized. The fitting is carried out using SciPy in JupyterLab in two sequential steps. First, each individual scan from a data set is fit to eq 6 with every parameter free to be optimized. As the phase of cosine functions can be rigorously compared only within a set of cosines with precisely the same frequency, the patterns are then fit a second time with f held at the average of all of the f values from the data set, and these final parameters are subsequently analyzed. As the signal-to-noise ratio of the interference patterns is high, the difference in

the relevant parameters between these two steps is generally <~0.5%.

By comparing eqs 5 and 6, it can be seen that $E_{sig} \propto A$. We do not attempt to deduce the absolute phase of the SHG signal and only interpret its changes in phase. Because φ_{LO} is constant and φ_{PSU} is varied in the same manner in each scan, changes in φ_{fit} must originate from changes in φ_{sig}, i.e., $\Delta\varphi_{fit} = \Delta\varphi_{sig}$. To move from $\Delta\varphi_{sig}$ to φ_{sig}, the phase of the sample under a specific condition must be known (or assumed). We assume that at 100 mM NaCl $\varphi_{sig} = 0°$ as $\chi^{(2)}$ and $\chi^{(3)}$ are purely real and at 100 mM NaCl the Debye length is sufficiently short such that φ_{DC} is near 0°. The sign of φ depends on the sign convention of the z-axis, a point of disagreement in the literature.[10] We assume that φ_{DC} is positive; therefore, we use the absolute value of φ extracted from the fits. We additionally place $\chi^{(2)}$ and $\chi^{(3)}\Phi(0)$ on the positive real axis of the complex plane, which places E_{sig} in the upper right quadrant in an Argand diagram.

ASSOCIATED CONTENT

$\textcircled{S}$ Supporting Information

The Supporting Information is available free of charge on the ACS Publications website at DOI: 10.1021/acs.jp-clett.9b00727.

> Derivation of eqs 2 and 3, calculation of wavevector mismatch, calculation of spatial and temporal overlap, SHG control studies, fit parameter from Figure 2A, and experimental setup (PDF)

AUTHOR INFORMATION

Corresponding Author
*E-mail: geigerf@chem.northwestern.edu.

ORCID
Paul E. Ohno: 0000-0003-4192-1888
HanByul Chang: 0000-0003-0270-7336
Austin P. Spencer: 0000-0003-4043-2062
Yangdongling Liu: 0000-0003-2750-9360
Hong-fei Wang: 0000-0001-8238-1641
Franz M. Geiger: 0000-0001-8569-4045

Author Contributions

P.E.O. and F.M.G. conceived of the idea. P.E.O., A.P.S., and F.M.G. designed the instrument. P.E.O. and H.B.C. collected the data. P.E.O., H.B.C., A.P.S., Y.L., M.D.B., H.-f.W., and F.M.G. analyzed the data. The manuscript was written with substantial input from all authors.

Notes

The authors declare no competing financial interest.

ACKNOWLEDGMENTS

■ REFERENCES

(1) Ong, S. W.; Zhao, X. L.; Eisenthal, K. B. Polarization of Water Molecules at a Charged Interface: Second Harmonic Studies of the Silica/Water Interface. *Chem. Phys. Lett.* **1992**, *191*, 327−335.

(2) Du, Q.; Freysz, E.; Shen, Y. R. Vibrational Spectra of Water Molecules at Quartz/Water Interfaces. *Phys. Rev. Lett.* **1994**, *72*, 238−241.

(3) Wang, H.; Yan, E. C. Y.; Borguet, E.; Eisenthal, K. B. Second Harmonic Generation from the Surface of Centrosymmetric Particles in Bulk Solution. *Chem. Phys. Lett.* **1996**, *259*, 15−20.

(4) Shen, Y. R.; Ostroverkhov, V. Sum-Frequency Vibrational Spectroscopy on Water Interfaces: Polar Orientation of Water Molecules at Interfaces. *Chem. Rev.* **2006**, *106*, 1140−1154.

(5) Eisenthal, K. B. Second Harmonic Spectroscopy of Aqueous Nano- and Microparticle Interfaces. *Chem. Rev.* **2006**, *106*, 1462−1477.

(6) Wen, Y.-C.; Zha, S.; Liu, X.; Yang, S.; Guo, P.; Shi, G.; Fang, H.; Shen, Y. R.; Tian, C. Unveiling Microscopic Structures of Charged Water Interfaces by Surface-Specific Vibrational Spectroscopy. *Phys. Rev. Lett.* **2016**, *116*, 016101.

(7) Gonella, G.; Lütgebaucks, C.; de Beer, A. G. F.; Roke, S. Second Harmonic and Sum Frequency Generation from Aqueous Interfaces Is Modulated by Interference. *J. Phys. Chem. C* **2016**, *120*, 9165−9173.

(8) Al-Abadleh, H. A.; Mifflin, A. L.; Bertin, P. A.; Nguyen, S. T.; Geiger, F. M. Control of Carboxylic Acid and Ester Groups on Chromium (VI) Binding to Functionalized Fused Silica/Water Interfaces Studied by Second Harmonic Generation. *J. Phys. Chem. B* **2005**, *109*, 9691−9702.

(9) Al-Abadleh, H. A.; Mifflin, A. L.; Musorrafiti, M. J.; Geiger, F. M. Kinetic Studies of Chromium (VI) Binding to Carboxylic Acid- and Methyl Ester-Functionalized Silica/Water Interfaces Important in Geochemistry. *J. Phys. Chem. B* **2005**, *109*, 16852−16859.

(10) Joutsuka, T.; Hirano, T.; Sprik, M.; Morita, A. Effects of Third-Order Susceptibility in Sum Frequency Generation Spectra: A Molecular Dynamics Study in Liquid Water. *Phys. Chem. Chem. Phys.* **2018**, *20*, 3040−3053.

(11) Schaefer, J.; Gonella, G.; Bonn, M.; Backus, E. H. G. Surface-Specific Vibrational Spectroscopy of the Water/Silica Interface: Screening and Interference. *Phys. Chem. Chem. Phys.* **2017**, *19*, 16875−16880.

(12) Jena, K. C.; Covert, P. A.; Hore, D. K. The Effect of Salt on the Water Structure at a Charged Solid Surface: Differentiating Second- and Third-Order Nonlinear Contributions. *J. Phys. Chem. Lett.* **2011**, *2*, 1056−1061.

(13) Jena, K. C.; Hore, D. K. Variation of Ionic Strength Reveals the Interfacial Water Structure at a Charged Mineral Surface. *J. Phys. Chem. C* **2009**, *113*, 15364−15372.

(14) Covert, P. A.; Jena, K. C.; Hore, D. K. Throwing Salt into the Mix: Altering Interfacial Water Structure by Electrolyte Addition. *J. Phys. Chem. Lett.* **2014**, *5*, 143−148.

(15) Darlington, A. M.; Jarisz, T. A.; Dewalt-Kerian, E. L.; Roy, S.; Kim, S.; Azam, M. S.; Hore, D. K.; Gibbs, J. M. Separating the pH-Dependent Behavior of Water in the Stern and Diffuse Layers with Varying Salt Concentration. *J. Phys. Chem. C* **2017**, *121*, 20229.

(16) Dewan, S.; Yeganeh, M. S.; Borguet, E. Experimental Correlation between Interfacial Water Structure and Mineral Reactivity. *J. Phys. Chem. Lett.* **2013**, *4*, 1977−1982.

(17) Darlington, A. M.; Jarisz, T. A.; DeWalt-Kerian, E. L.; Roy, S.; Kim, S. H.; Azam, M. S.; Hore, D. K.; Gibbs, J. M. Separating the Ph-Dependent Behavior of Water in the Stern and Diffuse Layers with Varying Salt Concentration. *J. Phys. Chem. C* **2017**, *121*, 20229−20241.

(18) Garcia Rey, N.; Weissenborn, E.; Schulze-Zachau, F.; Gochev, G.; Braunschweig, B. Quantifying Double-Layer Potentials at Liquid−Gas Interfaces from Vibrational Sum-Frequency Generation. *J. Phys. Chem. C* **2019**, *123*, 1279.

(19) Ohno, P. E.; Saslow, S. A.; Wang, H.-f.; Geiger, F. M.; Eisenthal, K. B. Phase-Referenced Nonlinear Spectroscopy of the α-Quartz/Water Interface. *Nat. Commun.* **2016**, *7*, 13587.

(20) Zhao, X.; Ong, S.; Wang, H.; Eisenthal, K. B. New Method for Determination of Surface pK_a Using Second Harmonic Generation. *Chem. Phys. Lett.* **1993**, *214*, 203−207.

(21) Zhao, X.; Ong, S.; Eisenthal, K. B. Polarization of Water Molecules at a Charged Interface. Second Harmonic Studies of Charged Monolayers at the Air/Water Interface. *Chem. Phys. Lett.* **1993**, *202*, 513−20.

(22) Hayes, P. L.; Malin, J. N.; Jordan, D. S.; Geiger, F. M. Get Charged Up: Nonlinear Optical Voltammetry for Quantifying the Thermodynamics and Electrostatics of Metal Cations at Aqueous/Oxide Interfaces. *Chem. Phys. Lett.* **2010**, *499*, 183−192.

(23) Geiger, F. M. Second Harmonic Generation, Sum Frequency Generation, and $\chi^{(3)}$: Dissecting Environmental Interfaces with a Nonlinear Optical Swiss Army Knife. *Annu. Rev. Phys. Chem.* **2009**, *60*, 61−83.

(24) Ohno, P. E.; Wang, H.-f.; Geiger, F. M. Second-Order Spectral Lineshapes from Charged Interfaces. *Nat. Commun.* **2017**, *8*, 1032.

(25) Ohno, P. E.; Wang, H.-f.; Paesani, F.; Skinner, J. L.; Geiger, F. M. Second-Order Vibrational Lineshapes from the Air/Water Interface. *J. Phys. Chem. A* **2018**, *122*, 4457−4464.

(26) Doğangün, M.; Ohno, P. E.; Liang, D.; McGeachy, A. C.; Bé, A. G.; Dalchand, N.; Li, T.; Cui, Q.; Geiger, F. M. Hydrogen-Bond Networks near Supported Lipid Bilayers from Vibrational Sum Frequency Generation Experiments and Atomistic Simulations. *J. Phys. Chem. B* **2018**, *122*, 4870−4879.

(27) Joutsuka, T.; Morita, A. Electrolyte and Temperature Effects on Third-Order Susceptibility in Sum-Frequency Generation Spectroscopy of Aqueous Salt Solutions. *J. Phys. Chem. C* **2018**, *122*, 11407.

(28) Boamah, M. D.; Ohno, P. E.; Geiger, F. M.; Eisenthal, K. B. Relative Permittivity in the Electrical Double Layer from Nonlinear Optics. *J. Chem. Phys.* **2018**, *148*, 222808.

(29) Geiger, F. M.; Ohno, P. E.; Wang, H.-f.; Eisenthal, K. B. *Optical Quantification of Interfacial Charge States.* U.S. Patent 20180164657, 2016.

(30) Fu, L.; Chen, S.-L.; Wang, H.-F. Validation of Spectra and Phase in Sub-1 cm^{-1} Resolution Sum-Frequency Generation Vibrational Spectroscopy through Internal Heterodyne Phase-Resolved Measurement. *J. Phys. Chem. B* **2016**, *120*, 1579−1589.

(31) Kemnitz, K.; Bhattacharyya, K.; Hicks, J. M.; Pinto, G. R.; Eisenthal, B.; Heinz, T. F. The Phase of Second-Harmonic Light Generated at an Interface and Its Relation to Absolute Molecular Orientation. *Chem. Phys. Lett.* **1986**, *131*, 285−290.

(32) Chang, R. K.; Ducuing, J.; Bloembergen, N. Relative Phase Measurement between Fundamental and Second-Harmonic Light. *Phys. Rev. Lett.* **1965**, *15*, 6−8.

(33) Stolle, R.; Marowsky, G.; Schwarzberg, E.; Berkovic, G. Phase Measurements in Nonlinear Optics. *Appl. Phys. B: Laser Opt.* **1996**, *63*, 491−498.

(34) Hicks, J. M.; Kemnitz, K.; Eisenthal, K. B.; Heinz, T. F. Studies of Liquid Surfaces by Second Harmonic Generation. *J. Phys. Chem.* **1986**, *90*, 560−562.

(35) Thiansathaporn, P.; Superfine, R. Homodyne Surface Second-Harmonic Generation. *Opt. Lett.* **1995**, *20*, 545−547.

(36) Lu, R.; Rao, Y.; Zhang, W.-k.; Wang, H.-f. Phase Measurement in Nonlinear Optics of Molecules at Air/Water Interface with Femtosecond Laser Pulses. *Proc. SPIE* **2002**, *4812*, 115−124.

(37) Tyson, A. L.; Woods, D. A.; Verlet, J. R. R. Time-Resolved Second Harmonic Generation with Single-Shot Phase Sensitivity. *J. Chem. Phys.* **2018**, *149*, 204201.

(38) Nowakowski, P. J.; Woods, D. A.; Bain, C. D.; Verlet, J. R. R. Time-Resolved Phase-Sensitive Second Harmonic Generation Spectroscopy. *J. Chem. Phys.* **2015**, *142*, 084201.

(39) Schwarzberg, E.; Berkovic, G.; Marowsky, G. Nonlinear Interferometry and Phase Measurements for Surface Second-Harmonic Generation in a Dispersive Geometry. *Appl. Phys. A: Solids Surf.* **1994**, *59*, 631−637.

(40) Mifflin, A. L.; Musorrafiti, M. J.; Konek, C. T.; Geiger, F. M. Second Harmonic Generation Phase Measurements of Cr(VI) at a Buried Interface. *J. Phys. Chem. B* **2005**, *109*, 24386−24390.

(41) Achtyl, J. L.; Vlassiouk, I. V.; Fulvio, P. F.; Mahurin, S. M.; Dai, S.; Geiger, F. M. Free Energy Relationships in the Electrical Double Layer over Single-Layer Graphene. *J. Am. Chem. Soc.* **2013**, *135*, 979−981.

(42) Langmuir, D. *Aqueous Environmental Chemistry*; Prentice Hall: Upper Saddle River, NJ, 1997.

(43) Dreier, L. B.; Bernhard, C.; Gonella, G.; Backus, E. H. G.; Bonn, M. Surface Potential of a Planar Charged Lipid−Water Interface. What Do Vibrating Plate Methods, Second Harmonic and Sum Frequency Measure? *J. Phys. Chem. Lett.* **2018**, *9*, 5685−5691.

(44) Hendrickx, E.; Clays, K.; Persoons, A. Hyper-Rayleigh Scattering in Isotropic Solution. *Acc. Chem. Res.* **1998**, *31*, 675−683.

(45) Ciddor, P. E. Refractive Index of Air: New Equations for the Visible and near Infrared. *Appl. Opt.* **1996**, *35*, 1566−1573.